energies

MDPI

Article

A Coordinated Emergency Frequency Control Strategy Based on Output Regulation Approach for an Isolated Industrial Microgrid

Xin Ding [1,*] and Sujie Zhang [2,3]

[1] School of Mechanical Engineering, University of Shanghai for Science and Technology, Shanghai 200093, China
[2] State Grid Shanghai Municipal Electric Power Company, Shanghai 200122, China; zhangsujiesgcc@163.com
[3] College of Electrical Engineering, Shanghai University of Electric Power, Shanghai 200090, China
* Correspondence: dingxin2016@whu.edu.cn

Abstract: Constructing isolated industrial microgrids with wind power is beneficial for improving the economic benefits of high-energy-consuming production, such as the electrolytic aluminum industry. Due to the specialized structure of industrial microgrids and the unique characteristics of the electrolytic aluminum load (EAL), the common emergency frequency control methods do not apply to the specific operational requirements of isolated industrial microgrids. Since EALs have huge regulating capacities and fast responses, this paper proposes a coordinated emergency frequency control scheme to deal with power disturbances in isolated industrial microgrids. The coordinated frequency control model of an industrial microgrid considering demand-side participation is derived. With the help of output regulation theory, a practical, feasible coordinated frequency controller is designed by introducing frequency deviation and power disturbance as feedback control signals. The proposed control scheme achieves reserve power distribution between the generation and demand sides. The microgrid frequency can be maintained within a permitted range in the presence of large power imbalances. The simulation results conducted in an actual isolated industrial microgrid validate the effectiveness and dynamic performance of the proposed control scheme.

Keywords: frequency control; isolated industrial microgrid; electrolytic aluminum; output regulation; wind power

check for updates

Citation: Ding, X.; Zhang, S. A Coordinated Emergency Frequency Control Strategy Based on Output Regulation Approach for an Isolated Industrial Microgrid. *Energies* **2024**, *17*, 5217. https://doi.org/10.3390/en17205217

Academic Editor: Muhammad Akmal

Received: 28 September 2024
Revised: 15 October 2024
Accepted: 19 October 2024
Published: 20 October 2024

Copyright: © 2024 by the authors. Licensee MDPI, Basel, Switzerland. This article is an open access article distributed under the terms and conditions of the Creative Commons Attribution (CC BY) license (https://creativecommons.org/licenses/by/4.0/).

1. Introduction

1.1. Background

In order to deal with environmental pollution and energy shortages, the Chinese government issued carbon peaking and carbon neutrality targets in 2020 [1]. Toward this end, carbon dioxide emissions in China will peak and stabilize by 2030, and carbon neutrality will be achieved by 2060 [2]. As a type of renewable energy, wind power generation plays an important role in Chinese low-carbon energy system construction, which has been developed rapidly in recent years [3]. According to the statistical reports issued by the National Energy Administration, by the end of 2023, the total wind power installed capacity in China had already reached to 441.3 GW, representing a 20.7% increase over the previous year [4]. Therefore, in order to obtain cheaper electricity, high-energy-consuming enterprises in China, such as the electrolytic aluminum industry, are gradually transiting production to regions with abundant thermal and wind power [5]. To facilitate wind power utilization and improve the economic profit of industries, isolated industrial microgrid construction is encouraged in China [6,7].

However, the isolated industrial microgrids are normally designed with simple electrical structures and disconnected from the utility grid, leading to smaller system inertia

than with large power grids. In addition, when the isolated industrial microgrid is integrated with a high proportion of wind power, the power system stability may be further deteriorated in terms of the large power disturbances and insufficient reserve capacity [8]. Therefore, emergency frequency control is one of the major technical issues for the operation of the isolated industrial microgrid [9].

1.2. Literature Review

The traditional emergency frequency control methods include the active power regulation of generators (primary and secondary frequency control) and load-shedding control strategies. In [10], an optimal primary frequency controller based on an adaptive optimal output–feedback approach was proposed to deal with uncertain disturbances in islanded microgrids. The authors of [11] presented a distributed robust secondary control approach to achieve frequency restoration and accurate active power sharing. The authors of [12] investigated a coordinated load-shedding control scheme to eliminate the power deficit for an islanded microgrid with distributed energy resources. In [13], the authors studied a deep learning-based load-shedding control strategy to determine the shedding action selection accurately. In addition, constructing an energy storage system (ESS) is a feasible solution to improve the stability of an isolated power grid with renewable energy. A joint frequency modulation control strategy combining wind farms and ESSs was employed to enhance the dynamic response characteristics under different wind speeds in [14]. The authors of [15] studied a variable droop strategy for an actual power grid with a battery ESS and evaluated its impact on the dynamic response.

Although the above literature is well studied, the common methods may not be particularly practical to guarantee the specific production requirements of the isolated industrial microgrid. The electrolytic aluminum load (EAL), as a type of energy-intensive industrial load, usually works as a whole part with an installed megawatt-class capacity, which means that the normal load-shedding strategy is not applicable for EALs.

As the time derivative of the power system frequency (df/dt), the rate of change of frequency (ROCOF) is important for qualifying the robustness of a power grid. Due to the small inertial of isolated industrial microgrids, extreme working scenarios, such as short faults on generators, may lead to the rapid decrease in the rate of change of frequency (ROCOF). Large-scale ESS construction will bring higher production costs for the high-energy-consuming enterprises, which is neither practical nor economical for isolated industrial microgrids.

Developing the regulating potential of EALs can be another feasible method, since the load control and demand response of EALs have been investigated by many research works. The authors of [16] studied the load control methods of the EAL based on its electrical model, such as controlling the transformer ratio and equivalent inductance of saturable reactors. By regulating the active power consumption of the EAL, the authors of [17] developed a frequency control method to eliminate the power imbalance in an isolated microgrid. In [18,19], the fast demand response provided by EALs was shown to smooth or track wind power fluctuations effectively by using tie-line power deviation as a feedback control signal. A hierarchical dispatch architecture of EALs and thermal generators in [20] was shown to provide secondary frequency auxiliary service for industrial microgrids. The aforementioned research works indicate that EALs are able to provide huge demand response in terms of emergency frequency control in isolated industrial microgrids.

Therefore, this paper aims to coordinate the generation and demand sides to achieve the emergency frequency control of isolated industrial microgrids with a high proportion of wind power. The traditional control strategies mainly focus on PI or PID controllers, which are incapable of achieving satisfactory effects. The PI control methods in [21,22] were unable to achieve zero-steady-error tracking in the presence of wind power fluctuations. Several research works applied model predictive control (MPC) methods to improve the dynamic performance. In [23], an MPC-based frequency controller was formulated to regulate the demand side and address the large power disturbance in microgrids. The

authors of [24] proposed an MPC-based demand-side management strategy to smooth distributed photovoltaic power fluctuations. Although MPC controllers are capable of achieving the required performance, the complexity of online optimization algorithms brings significant difficulties for practical applications.

On the other hand, frequency control issues have been formulated as output regulation problems by several works. The authors of [25] investigated a frequency and excitation voltage control scheme by applying regulator theory to achieve demand-side regulation. In [26], the authors proposed a voltage and frequency regulation strategy based on the output regulation approach to track voltage and frequency references accurately in terms of the occurrence of disturbance events. Motivated by the positive error tracking ability and the practical feasibility, this paper adopts output regulation theory to develop a coordinated emergency frequency control for isolated industrial microgrids.

1.3. Contributions

In order to address the frequency control issues in isolated industrial microgrids with a high penetration of wind power, this paper aims to investigate the regulation potential of EALs by developing a detailed control model. For the purpose of restoring frequency in the presence of active power disturbances caused by emergencies or wind power fluctuations, a coordinated frequency control scheme based on the output regulation approach is proposed to combine the thermal generators and EALs.

In summary, the main contributions of this work are summarized as follows:

1. The emergency frequency control issues in isolated aluminum production industrial microgrids are discussed in detail. The control model of EALs and the advantages of demand-side control in isolated industrial microgrids are also illustrated.
2. A coordinated frequency control model combining thermal generators and EALs is developed for emergency frequency regulation in the isolated industrial microgrid in the presence of low system inertia and insufficient reserve capacity.
3. The problem of emergency frequency control is formulated as an output regulation problem. With the help of the output regulation approach, a practically feasible frequency controller is investigated with the feedback control signals of frequency deviation and power disturbances, verifying that it increases the rapid frequency regulating capacity of isolated industrial microgrids.

1.4. Organization

The remainder of this paper is organized as follows. Section 2 describes the emergency frequency control issues in an actual isolated industrial microgrid with a high proportion of wind power. In Section 3, the coordinated frequency control model is developed, including the detailed control model of EALs. In Section 4, the output regulation theory is applied to derive solutions for coordinated frequency control problems and to implement the frequency control scheme. The simulation results and analyses are presented in Section 5. The conclusions are given in Section 6.

2. Emergency Frequency Control Issues in Isolated Industrial Microgrids

As a northern province in China, Inner Mongolia is abundant with coal and wind energy resources, which is attractive for high-energy-consuming industries due to the lower electricity price. Electrolytic aluminum enterprises in China are gradually transiting production to the northern areas with abundant renewable energy. The technical and economic assessment in [27] has revealed the economic efficiency and engineering feasibility of constructing isolated industrial aluminum production microgrids. Thus, an actual industrial microgrid located in Inner Mongolia for aluminum production is selected as the study case, with the grid configuration shown in Figure 1. The main components of the industrial microgrid include generation sources, transformers, transmission lines, and loads. The generation sources consist of eight self-owned thermal generators (G1–G8) with a total installed capacity of 1800 MW and two 400-MW wind farms (WF1–WF2). Since the

isolated industrial microgrid is constructed specifically for aluminum production, the main loads in the microgrid include three aluminum production lines (EAL1–EAL3) and regular heating loads. The loads are supplied by the thermal generators and wind farms directly via transformers and transmission lines. The detailed installed capacity of the thermal generators and wind farms, and the power demand of the loads, are listed in Tables 1 and 2, respectively.

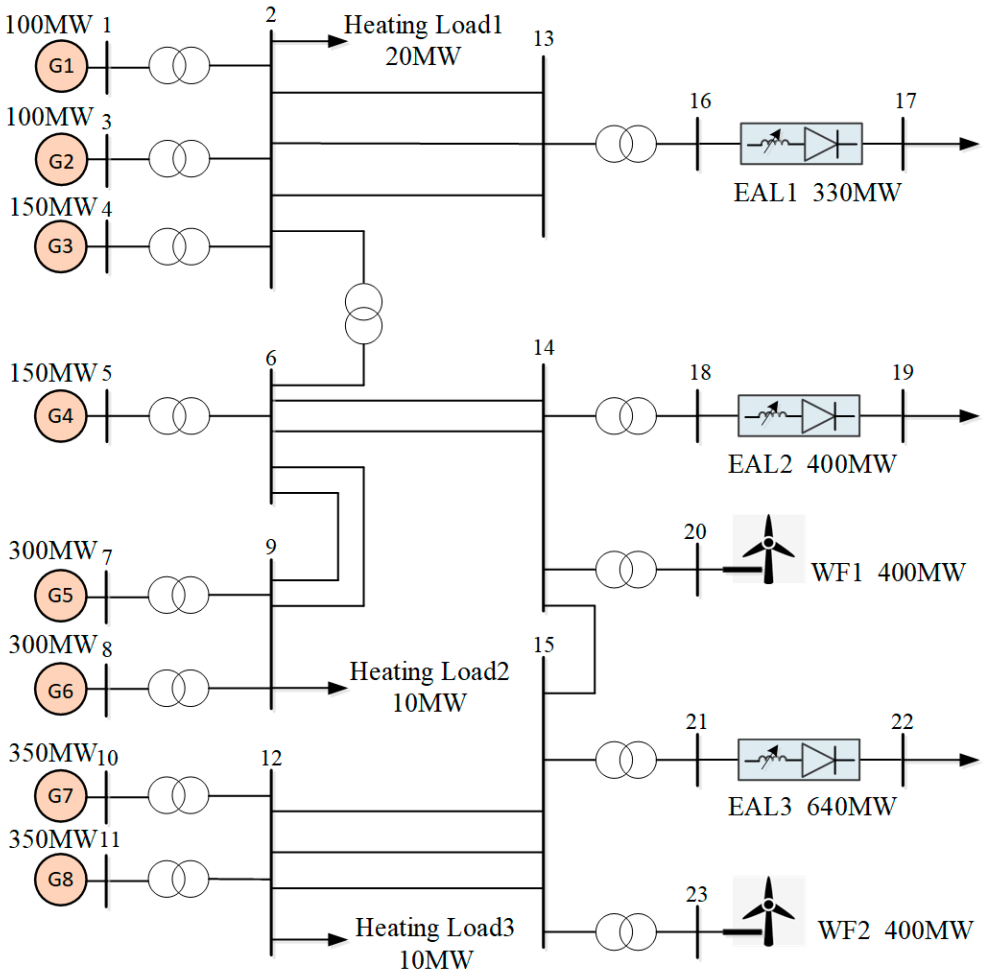

Figure 1. The structure of the actual isolated industrial microgrid for aluminum production.

Table 1. The installed capacity of thermal generators and wind farms.

Generators/Wind Farms	G1/G2	G3/G4	G5/G6	G7/G8	WF1/WF2
Installed Capacity (MW)	100	150	300	350	400

Table 2. The power demand of the EALs and heating loads.

EALs/Heating Loads	EAL1	EAL2	EAL3	Heating Load1	Heating Load2	Heating Load3
Power Demand (MW)	330	400	640	20	10	10

The isolated industrial microgrid operation is supposed to meet the security requirements of the power system, such as the "N-1" principle. The microgrid is supposed to have a sufficient reserve capacity to cope with active shortages and maintain a stable frequency when any one of the generation units is out of service. Generally, the primary

frequency control reserve from thermal generators is set as 5% of the installed capacity, which means 90 MW in total for the power reserve. Table 3 lists a typical working situation for thermal generators and wind farms. For instance, when the thermal generator G5 is out of service because of short-circuit faults, the huge active power shortage of 170.2 MW in the industrial microgrid is much higher than the primary frequency reserve from the rest of the generators at 75 MW. The frequency nadir, representing the lowest point of the frequency when a power disturbance occurs, is an essential critical indicator for evaluating the power system stability.

Table 3. The output power of thermal generators and wind farms in a typical working situation.

Generation Units	G1/G2	G3/G4	G5/G6	G7/G8	WF1/WF2
Output Power (MW)	60.4	85.4	170.2	191.5	212.8

The generator G5 is tripped off from the microgrid at t = 2 s, leading to the frequency dropping down to the nadir of 48.48 Hz within 3 s (with the ROCOF of 4.45 Hz/s at the beginning of the emergency) and remaining steady at 49.5 Hz in the end, as shown in Figure 2.

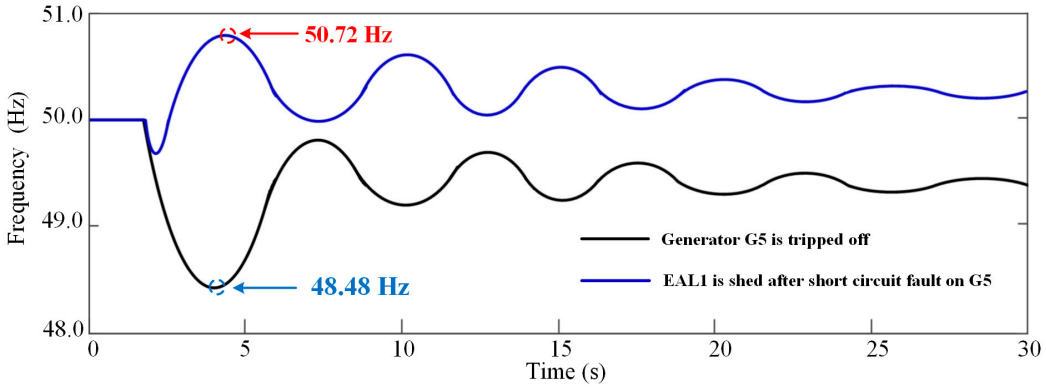

Figure 2. The frequency curves of different situations in the isolated industrial microgrid.

However, the traditional load-shedding strategy is not practical in this industrial microgrid because the EAL works as a whole part. The active power demand of three electrolytic aluminum production lines is listed in Table 2, demonstrating that the capacity of a single EAL is much larger than that of a single generator. Figure 2 demonstrates the frequency response when applying the load-shedding strategy. EAL1 is shed at 0.5 s after generator G5 being tripped off, leading the frequency rising to the peak of 50.72 Hz, which may activate the over-frequency protection of the generators and result in the further collapse of the system frequency. Obviously, it is difficult for the common methods, such as the primary frequency control and load-shedding strategy, to maintain the frequency stability in isolated industrial microgrids for the following reasons:

1. The reserve capacity from the thermal generators is insufficient for the large power imbalance caused by emergency faults. In addition, installing a high penetration of wind power (up to about 31%) and disconnecting from the utility power grid would further decrease the inertia of the microgrid.
2. Due to the special structure of the industrial microgrid, the installed capacity of a single generator or EAL is relatively huge compared with the total power demand capacity, which brings difficulties in achieving an active power balance with the common methods.

On the other hand, with the integration of a high penetration of wind power, the inertia of the isolated power system would decrease and the frequency stability characteristics would worsen. The active power imbalances caused by wind power fluctuation may result

in rapid frequency change. The intensive wind fluctuation can reach up to ±15% of the installed capacity of wind farms in seconds. For cost reasons, wind turbine generators are generally encouraged to operate in maximum power point tracking (MPPT) mode, which provides no extra frequency regulation reserve. Except for the insufficient reserve capacity, the regulating ratio of the thermal generators may have difficulty in covering the intensive wind power fluctuation. Thus, integrating a high penetration of wind power in isolated industrial microgrids also brings severe frequency stability issues.

As a type of high-energy-consuming industrial load, the EAL has been proven to provide regulation potential, as mentioned in Section 1. Previous studies have also illustrated the control methods and regulation ability of EALs [16–20]. EALs are shown to provide regulation characteristics of a considerable capacity and a fast response, which will be discussed in detail in Section 3. Therefore, instead of traditional load-shedding strategies, the active power demand of EALs can be controlled accurately to provide reserve capacity to compensate for power imbalances. In view of the outcomes of the common control methods analyzed above, we propose a coordinated emergency frequency control scheme in this paper to combine the generation and demand sides in the presence of emergencies and intensive wind fluctuation scenarios. To obtain the theoretically feasible controller and desirable control effect, the output regulation theory will be applied to design the coordinate frequency control scheme in Section 4, aiming to achieve stable frequency recovery in the presence of large and intensive power disturbances.

3. Isolated Industrial Microgrid Modeling

3.1. Model and Control of EAL

In the case of the isolated industrial microgrid, the EAL is selected as the controlled plant for the demand-side control. Modern aluminum smelting production is usually generated in the electrolytic cell by using the Hall–Héroult Process to produce pure aluminum [28]. The high direct current (up to several hundred kiloamperes) is passed through to the electrolyzer and the aluminum oxide is smelted at high temperatures (over 950 °C). Then, the pure aluminum is decomposed between the carbon and aluminum electrodes.

The electrical diagram and equivalent circuit of the EAL have been investigated in detail in [16], which is shown in Figure 3. The EAL production line includes the AC bus, on-load tap changer (OLTC) transformer, rectification system, DC bus, and electrolyzer. All of the electrolyzers in a single EAL production line are connected in a series and supplied by the DC bus voltage U_{DC}. The AC bus voltage U_{AC} is regulated and rectified by the OLTC transformers (k_T is the transformer ratio) and rectification system. U_{SR} is the voltage drop on saturable reactors, with a normal working value of around 40 V. In [17], the electrolyzer is represented by a back electromotive force (EMF) E and a constant resistance R.

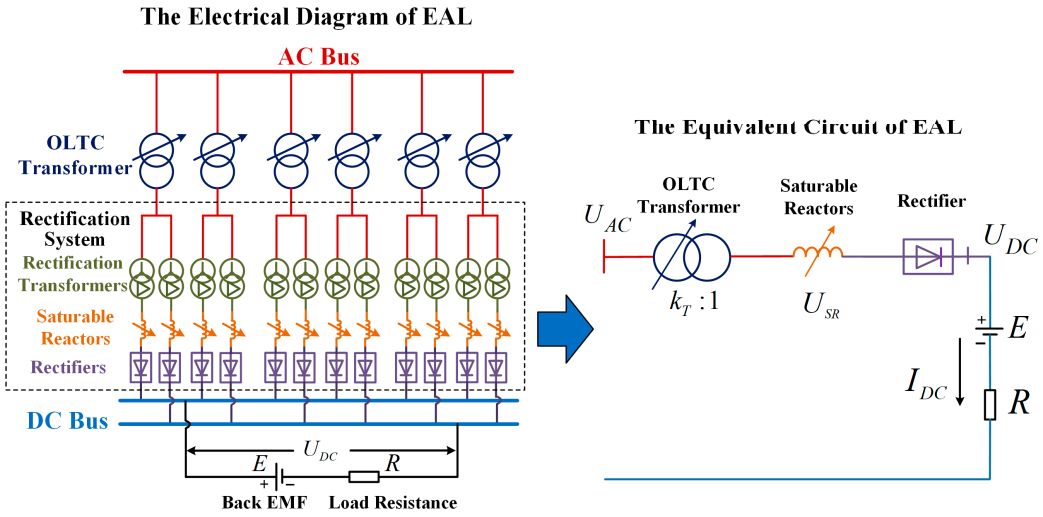

Figure 3. The electrical diagram and equivalent circuit of the EAL.

The DC current I_{DC} in the electrolyzer is calculated as [17]

$$I_{DC} = \frac{U_{DC} - E}{R} = \frac{1.35(U_{AC}/k_T - U_{SR}) - E}{R} \quad (1)$$

Thus, the active power consumption of the EAL P_{EAL} is calculated as

$$P_{EAL} = U_{DC} I_{DC} = (I_{DC} R + E) I_{DC} \quad (2)$$

In actual production, P_{EAL} can be regulated by the following two methods: (1) regulating the OLTC transformer ratio k_T; (2) changing the voltage drop on the saturable reactors U_{SR}. In practice, changing the voltage drop on the saturable reactors is preferable to regulating the OLTC transformer ratio for the following reasons:

1. Regulating the OLTC transformer ratio k_T is realized by changing the transformer tap changer positions, which takes minutes for one mechanical operation. In addition, the transformer tap changers are not allowed to be adjusted frequently for prolonging the life-span. Conversely, changing the voltage drop on saturable reactors U_{SR} with the electronic control only takes less than one second, which is much faster than the mechanical control, demonstrating the great advantages of the rapid response (millisecond level) in the presence of emergencies and wind power fluctuations.
2. Generally, the transformer tap changers have only five positions (i.e., $k_T = 1 \pm 2 \times 2.5\%$), indicating the step regulation on the active power control, while regulating the voltage drop on saturable reactors presents a much subtler way to achieve continuous regulation.

In [29], it was proven that P_{EAL} can be regulated from over -0.9 p.u. to 1.05 p.u. of the load capacity by controlling U_{SR} within its working limits (10–70 V), which means a considerable regulation capacity in terms of the megawatt-level loads. Thus, it is more feasible to adjust U_{SR} to achieve a rapid regulation.

Combining Equations (1) and (2), the relations between the active power deviation of the EAL ΔP_{EAL} and DC current deviation ΔI_{DC} voltage drop on saturable reactors ΔU_{SR} can be deduced as follows:

$$\Delta P_{EAL} = R\Delta I_{DC}^2 + R(I_{DC0} + E)\Delta I_{DC} \quad (3)$$

$$\Delta P_{EAL} = \frac{1.83\Delta U_{SR}^2 + (1.35E - 2.7\, U_{DC0})\Delta U_{SR}}{R} \quad (4)$$

where I_{DC0} and U_{DC0} are the initial values of the direct current and DC bus voltage.

Taking an actual EAL of 330 MW in [29] as an example, I_{DC0} and U_{DC0} are equal to 326.1 kA and 1.012 kV, respectively. E and R are equal to 354.6 V and 2.016 mΩ based on the field experiments. Thus, Equations (3) and (4) can be calculated as

$$\Delta P_{EAL} = 0.002016\Delta I_{DC}^2 + 1315.6\Delta I_{DC},\ \Delta P_{EAL} = 907\Delta U_{SR}^2 - 1.118 \times 10^6 \Delta U_{SR}$$

Obviously, the quadratic terms (ΔI_{DC}^2 and ΔU_{DC}^2) contain a slight proportion of and present a negligible influence on the value of ΔP_{EAL}. Thus, Equations (3) and (4) can be further simplified as

$$\Delta P_{EAL} \approx K_{PI}\Delta I_{DC},\ K_{PI} = R(I_{DC0} + E) \quad (5)$$

$$\Delta P_{EAL} \approx K_{PV}\Delta U_{SR},\ K_{PV} = (1.35E - 2.7\, U_{DC0})/R \quad (6)$$

where K_{PI} and K_{PV} are the gain coefficients, which are determined by the initial values of the EALs.

Based on the discussion above, the demand-side control model of the EAL is demonstrated in Figure 4. The control model includes the transfer functions of the electrolyzer and the saturable reactor control circuits. The time constants T_{ES} and T_{SR} are the response time of the electrolyzer and the saturable reactor control circuits, which can be approximated

based on the dynamic response of each section. K_p, K_i, and K_{SR} are the gain coefficients in the saturable reactor control circuits. $\Delta U_{SR\max}$ and $\Delta U_{SR\min}$ are the upper and lower limits for ΔU_{SR}. The demand-side control model indicates that the active power consumption changes in the EAL ΔP_{EAL} can be regulated by providing the active power reference ΔP_{EALref}. Furthermore, the dynamic response of the demand-side control can be calculated as Equation (7), as follows:

$$G_{EAL}(s) = \frac{K_{PV}K_{SR}(K_i + sK_p)}{sK_{PI}(1+sT_{ES})(1+sT_{SR})} \tag{7}$$

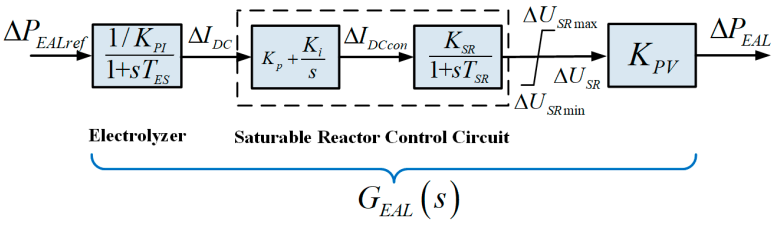

Figure 4. The demand-side control model on the EAL.

3.2. Coordinated Emergency Frequency Control Model of Isolated Industrial Microgrid

In this paper, a coordinated emergency frequency control model is proposed to combine the generation and demand side to balance the active power disturbance in the isolated industrial microgrid, and, if possible, to recover the frequency deviation Δf back to zero. Considering that the isolated industrial microgrid contains m thermal generators and n EALs, the block diagram of the coordinated emergency frequency control model is given as Figure 5. M and D are the equivalent constants of the inertia and load damping in the isolated industrial microgrid, respectively. ΔP_D is the active power disturbances, such as power imbalances or wind power fluctuations. For the i-th thermal generator and j-th EAL, the notations are presented in Table 4.

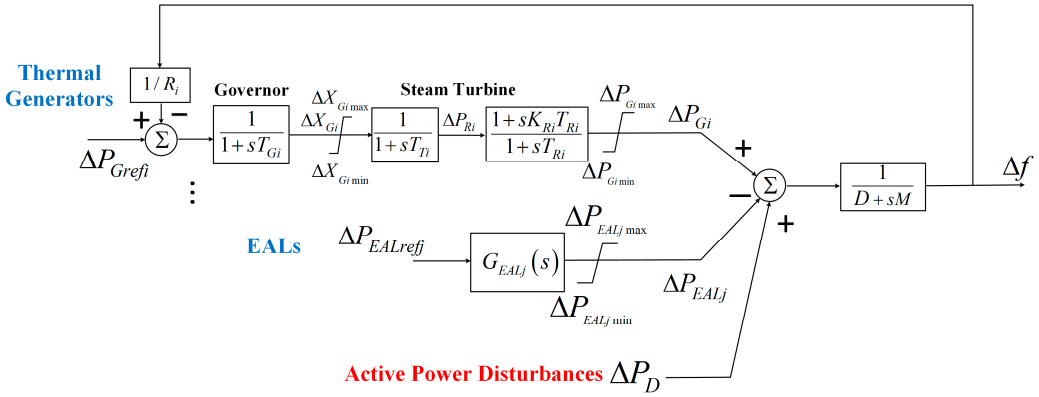

Figure 5. Coordinated emergency frequency control model of the isolated industrial microgrid.

Based on the block diagram in Figure 5, the state space model of the isolated industrial microgrid is described as

$$\begin{cases} \Delta\dot{f} = -\frac{D}{M}\Delta f + \frac{1}{M}\Delta P_{Gi} - \frac{1}{M}\Delta P_{EALj} + \frac{1}{M}\Delta P_D \\ \Delta\dot{P}_{Gi} = -\frac{1}{T_{Ri}}\Delta P_{Gi} + \left(\frac{1}{T_{Ri}} - \frac{K_{Ri}}{T_{Ti}}\right)\Delta P_{Ri} + \frac{K_{Ri}}{T_{Ti}}\Delta X_{Gi} \\ \Delta\dot{P}_{Ri} = -\frac{1}{T_{Ti}}\Delta P_{Ri} + \frac{1}{T_{Ti}}\Delta X_{Gi} \\ \Delta\dot{X}_{Gi} = -\frac{1}{T_{Gi}R_i}\Delta f - \frac{1}{T_{Gi}}\Delta X_{Gi} + \frac{1}{T_{Gi}}\Delta P_{Grefi} \\ \Delta\dot{I}_{DCj} = -\frac{1}{T_{ESj}}\Delta I_{DCj} + \frac{1}{T_{ESj}K_{PIj}}\Delta P_{EALrefj} \\ \Delta\dot{I}_{DCconj} = \left(K_{ij} - \frac{K_{pj}}{T_{ESj}}\right)\Delta I_{DCj} + \frac{K_{pj}}{T_{ESj}K_{PIj}}\Delta P_{EALrefj} \\ \Delta\dot{P}_{EALj} = \frac{K_{PVj}K_{SRj}}{T_{SRj}}\Delta I_{DCconj} - \frac{1}{T_{SRj}}\Delta P_{EALj} \end{cases} \tag{8}$$

Since the aim of the proposed coordinated emergency frequency control strategy is to eliminate the frequency deviation, the output of control system $\boldsymbol{y}$ is given as

$$\boldsymbol{y} = \Delta f \tag{9}$$

Combining Equations (8) and (9), the coordinated emergency frequency control model can be summarized as

$$\begin{cases} \dot{\boldsymbol{x}} = \boldsymbol{A}\boldsymbol{x} + \boldsymbol{B}\boldsymbol{u} + \boldsymbol{P}\boldsymbol{d} \\ \boldsymbol{y} = \boldsymbol{C}\boldsymbol{x} \end{cases} \tag{10}$$

where $\boldsymbol{x}$, $\boldsymbol{u}$, $\boldsymbol{y}$, and $\boldsymbol{d}$ are the variables of the system state, control input, output, and disturbance, respectively, expressed as in Equation (11). The detailed expressions of the matrices $\boldsymbol{A}$, $\boldsymbol{B}$, $\boldsymbol{C}$, and $\boldsymbol{P}$ can be deduced according to Equations (8) and (9).

$$\begin{gathered} \boldsymbol{x} = \left[\Delta f, \boldsymbol{\Delta P_{Gi}}, \boldsymbol{\Delta P_{Ri}}, \boldsymbol{\Delta X_{Gi}}, \boldsymbol{\Delta I_{DCj}}, \boldsymbol{\Delta I_{DCconj}}, \boldsymbol{\Delta P_{EALj}}\right]^{\mathrm{T}} \in R^{(1+3i+3j)\times 1} \\ \boldsymbol{u} = \left[\boldsymbol{\Delta P_{Grefi}}, \boldsymbol{\Delta P_{EALrefj}}\right]^{\mathrm{T}} \in R^{(i+j)\times 1}, \ \boldsymbol{d} = \Delta P_D \end{gathered} \tag{11}$$

Therefore, the space state equations of the coordinated frequency control model of the isolated industrial microgrid are described as Equations (10) and (11). On the basis of that, the coordinated emergency frequency control strategy aims to increase the rapid frequency regulation ability and recover the frequency to the normal value when power disturbances exist.

Table 4. The notations in the coordinated emergency frequency control model.

Notation	Meaning
R_i	droop control coefficient
ΔX_{Gi}	valve position deviation
T_{Ri}	time constant of the reheater
ΔP_{Ri}	output power deviation of the reheater
K_{Ri}	turbine power fraction
ΔP_{Gi}	output power deviation of the steam turbine
$\Delta P_{Gimax}/\Delta P_{Gimin}$	maximal/minimal value of ΔP_{Gi}
T_{Gi}	time constant of the speed governor
T_{Ti}	time constant of the steam turbine
ΔP_{Grefi}	control input of the generator
ΔP_{EALj}	active power regulation of the EAL
$\Delta P_{EALjmax}/\Delta P_{EALjmin}$	maximal/minimal value of ΔP_{EALj}
$\Delta P_{EALrefj}$	control input of the EAL

4. Coordinated Emergency Frequency Control Through Output Regulation

4.1. Output Regulation via Error Feedback

In the presence of a power disturbance ΔP_D, the control objective of the coordinated emergency frequency control strategy is to regulate the active power output of the generators P_{Gi} and the power consumption of the EALs P_{EALj} to smooth ΔP_D. Thus, the

coordinated frequency control is formulated as an output regulation issue, which can be described with the following linearization form:

$$\begin{cases} \dot{x} = Ax + Bu + Pd \\ \dot{d} = Sd \\ e = y - y_r = Cx + Qd \end{cases} \tag{12}$$

The first equation represents the relation between the system state x, control input u, and external disturbance d. The second equation describes the characteristics of the exosystem with disturbances. The third equation defines an error variable e by introducing the output $y = Cx$ and the reference $y_r = Qd$. The detailed block diagram of the closed-loop control plant in Equation (12) is presented in Figure 6.

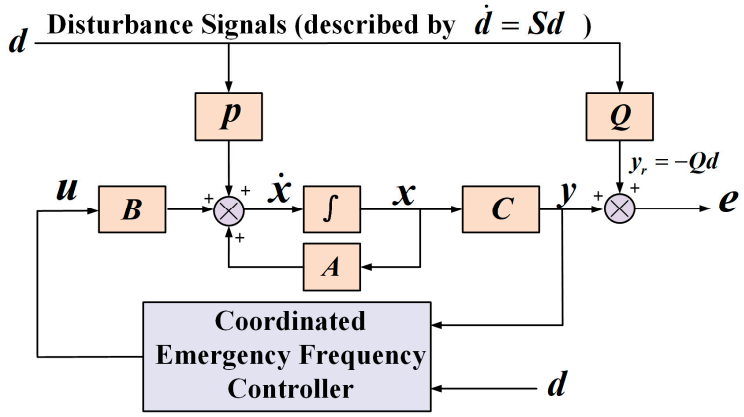

Figure 6. Block diagram of the coordinated emergency frequency control plant.

The coordinated emergency frequency controller aims to achieve error regulation and to maintain the system's internal stability. In other words, for the control system in Equation (12), find the gain matrices K and L, if possible, to design the full-information feedback controller as

$$u = Kx + Ld \tag{13}$$

The feedback controller in Equation (13) is supposed to satisfy the following two requirements:

(R1) Internal stability. When the disturbance $d = 0$, the closed-loop control system $\dot{x} = (A + BK)x$ is asymptotically stable, which means that all of the eigenvalues of $(A + BK)$ are on the open left-half plane;

(R2) Error regulation. When the disturbance $d \neq 0$, for every initial condition (x_0, d_0), the closed-loop control system achieves $\lim_{t\to\infty} e(t) = 0$.

In order to solve the output regulation issues, the following two assumptions must be satisfied at first:

(A1) All of the eigenvalues of the matrix S are supposed to be located on the closed right-half plane;

(A2) The matrices pair (A,B) is stabilizable.

Based on the regulator theory in [30], when the assumptions (A1) and (A2) are satisfied, the necessary and sufficient condition has been proven to solve the output regulation issues.

Proposition 1. *Under (A1) and (A2), the output regulation issues can be solvable by full-information feedback if and only if there exist matrices* Π *and* Γ*, which solve the following regulator equations:*

$$\begin{cases} \Pi S = A\Pi + B\Gamma + P \\ 0 = C\Pi + Q \end{cases} \tag{14}$$

The gain matrix $\boldsymbol{L}$ can be computed as follows by the matrices $\boldsymbol{\Pi}$ and $\boldsymbol{\Gamma}$:

$$\boldsymbol{L} = \boldsymbol{\Gamma} - K\boldsymbol{\Pi} \tag{15}$$

Consequently, the feedback controller in Equation (13) can be designed as

$$\boldsymbol{u} = \boldsymbol{Kx} + (\boldsymbol{\Gamma} - \boldsymbol{K\Pi})\boldsymbol{d} \tag{16}$$

Although the feedback controller can be constructed as Equation (16), it may be not feasible in practice because not all of the state variables $\boldsymbol{x}$ can be obtained as required. Thus, the feedback controller can be further refined by using only the measurable error signal $\boldsymbol{e}$. An observer is constructed to track $(\boldsymbol{x}, \boldsymbol{d})$ asymptotically based on the following assumption:

(A3) The matrices pair $\left(\begin{bmatrix} \boldsymbol{A} & \boldsymbol{P} \\ \boldsymbol{0} & \boldsymbol{S} \end{bmatrix}, \begin{bmatrix} \boldsymbol{C} & \boldsymbol{Q} \end{bmatrix}\right)$ is detectable.

Under (A3), the observer in the following equation is constructed to estimate $\boldsymbol{x}$ and $\boldsymbol{d}$ by using error signal $\boldsymbol{e}$:

$$\begin{bmatrix} \dot{\hat{\boldsymbol{x}}} \\ \dot{\hat{\boldsymbol{d}}} \end{bmatrix} = \left(\begin{bmatrix} \boldsymbol{A} & \boldsymbol{P} \\ \boldsymbol{0} & \boldsymbol{S} \end{bmatrix} - \begin{bmatrix} \boldsymbol{G}_1 \\ \boldsymbol{G}_2 \end{bmatrix} \begin{bmatrix} \boldsymbol{C} & \boldsymbol{Q} \end{bmatrix} \right) \begin{bmatrix} \hat{\boldsymbol{x}} \\ \hat{\boldsymbol{d}} \end{bmatrix} + \begin{bmatrix} \boldsymbol{G}_1 \\ \boldsymbol{G}_2 \end{bmatrix} \boldsymbol{e} + \begin{bmatrix} \boldsymbol{B} \\ \boldsymbol{0} \end{bmatrix} \tag{17}$$

The matrices pair $(\boldsymbol{G}_1, \boldsymbol{G}_2)$ is designed so that all of the eigenvalues of $\left(\begin{bmatrix} \boldsymbol{A} & \boldsymbol{P} \\ \boldsymbol{0} & \boldsymbol{S} \end{bmatrix} - \begin{bmatrix} \boldsymbol{G}_1 \\ \boldsymbol{G}_2 \end{bmatrix} \begin{bmatrix} \boldsymbol{C} & \boldsymbol{Q} \end{bmatrix} \right)$ are on the open left-half plane.

With the help of the observer in Equation (17), the error feedback controller can be designed with $\boldsymbol{\xi} = \mathrm{col}(\hat{\boldsymbol{x}}, \hat{\boldsymbol{d}})$ and the gain matrices $(\boldsymbol{F}, \boldsymbol{G}, \boldsymbol{H})$, given as

$$\begin{cases} \dot{\boldsymbol{\xi}} = \boldsymbol{F\xi} + \boldsymbol{Ge} \\ \boldsymbol{u} = \boldsymbol{H\xi} \end{cases} \tag{18}$$

The gain matrices $(\boldsymbol{F}, \boldsymbol{G}, \boldsymbol{H})$ can be deduced by replacing $(\boldsymbol{x}, \boldsymbol{d})$ in Equation (16) with $(\hat{\boldsymbol{x}}, \hat{\boldsymbol{d}})$ after solving Equation (14), with the following expressions:

$$\begin{gathered} \boldsymbol{F} = \begin{bmatrix} \boldsymbol{A} - \boldsymbol{G}_1\boldsymbol{C} + \boldsymbol{BK} & \boldsymbol{P} - \boldsymbol{G}_1\boldsymbol{Q} + \boldsymbol{B}(\boldsymbol{\Gamma} - \boldsymbol{K\Pi}) \\ -\boldsymbol{G}_2\boldsymbol{C} & \boldsymbol{S} - \boldsymbol{G}_2\boldsymbol{Q} \end{bmatrix} \\ \boldsymbol{G} = \begin{bmatrix} \boldsymbol{G}_1 \\ \boldsymbol{G}_2 \end{bmatrix} \quad \boldsymbol{H} = \begin{bmatrix} \boldsymbol{K} & (\boldsymbol{\Gamma} - \boldsymbol{K\Pi}) \end{bmatrix} \end{gathered} \tag{19}$$

By using the error signal, the feedback controller in Equation (18) is able to achieve the control requirements (R1) and (R2). On the basis of that, the control system output $\boldsymbol{y} = \boldsymbol{Cx}$ can be the controlled to follow the reference $\boldsymbol{y_r} = \boldsymbol{Qd}$ via error feedback.

4.2. Implementation of Coordinated Emergency Frequency Control Scheme

The design procedure of the coordinated emergency frequency control scheme based on the output regulation is presented as follows:

1. *Model the control plant*. At time t_k, the state variables $\boldsymbol{x}$, disturbance $\boldsymbol{d}$, and frequency deviation Δf in the isolated industrial microgrid are collected via the wide area measurement system (WAMS) [31]. The coordinated frequency control model that considers the generation and demand-side participation is constructed as in Equations (8)–(10).
2. *Check the assumptions* (A1)–(A3). Since the collected active power disturbance ΔP_D changes with the step signal at each sampling time, the value of ΔP_D is assumed as constant. Then, $\boldsymbol{d} = \Delta P_D$ satisfies $\dot{\boldsymbol{d}} = \boldsymbol{Sd} = \boldsymbol{0}$, which means that the exosystem is Poisson stable and the assumption (A1) holds in this work. (A2) and (A3) can be

checked by using the Popov–Belevitch–Hautus (PBH) test, with the rank conditions presented as

$$\begin{aligned} Rank\left(\begin{bmatrix}\lambda \boldsymbol{I_A} - \boldsymbol{A} & \boldsymbol{B}\end{bmatrix}\right) &= n_A \\ Rank\left(\begin{bmatrix}\mu \boldsymbol{I_{APS}} - \begin{bmatrix}\boldsymbol{A} & \boldsymbol{P} \\ \boldsymbol{0} & \boldsymbol{S}\end{bmatrix} \\ \begin{bmatrix}\boldsymbol{C} & \boldsymbol{Q}\end{bmatrix}\end{bmatrix}\right) &= n_{APS} \end{aligned} \tag{20}$$

where λ and μ are the eigenvalues of the matrices $\boldsymbol{A}$ and $\begin{bmatrix}\boldsymbol{A} & \boldsymbol{P} \\ \boldsymbol{0} & \boldsymbol{S}\end{bmatrix}$ sitting on the closed right-half plane. $\boldsymbol{I_A}$ and $\boldsymbol{I_{APS}}$ are the identity matrices, and n_A and n_{APS} are the dimensions, respectively.

3. *Select gain matrices*. Once the assumptions (A1)–(A3) hold, find a gain matrix $\boldsymbol{K}$, such that all of the eigenvalues of $\boldsymbol{A} + \boldsymbol{BK}$ are located on the left-half plane. A linear quadratic (LQ) method is applied in this work to obtain a reasonable gain matrix $\boldsymbol{K}$, achieving the control objectives with a satisfactory performance by the controllers. The cost function for the LQ method is given as follows:

$$\boldsymbol{J_{lq}} = \int_0^\infty \left(\boldsymbol{y}^{\mathrm{T}} \boldsymbol{Q_{lq}} \boldsymbol{y} \ + \boldsymbol{u}^{\mathrm{T}} \boldsymbol{R_{lq}} \boldsymbol{u}\right) \mathrm{d}t \tag{21}$$

The selection of the weighting matrices $\boldsymbol{Q_{lq}}$ and $\boldsymbol{R_{lq}}$ means a trade-off between the eliminating error (the frequency deviation Δf in this case) and optimizing the control performance on the thermal generators/EALs. Thus, the power system inertia and flexibility in designing the coordinated control scheme is judged and weighted by solving following equations and computing the gain matrix $\boldsymbol{K}$:

$$\boldsymbol{A}^{\mathrm{T}} \boldsymbol{P_{lq}} + \boldsymbol{P_{lq}^{\mathrm{T}}} \boldsymbol{A} - \boldsymbol{P_{lq}} \boldsymbol{B} \boldsymbol{R_{lq}^{-1}} \boldsymbol{B}^{\mathrm{T}} \boldsymbol{P_{lq}} + \boldsymbol{C}^{\mathrm{T}} \boldsymbol{Q_{lq}} \boldsymbol{C} \ = \ 0 \tag{22}$$

$$\boldsymbol{K} = -\boldsymbol{R_{lq}^{-1}} \boldsymbol{B}^{\mathrm{T}} \boldsymbol{P_{lq}} \tag{23}$$

4. Similarly, it is also supposed that the gain matrix $\boldsymbol{G}$ satisfies that all of the eigenvalues of $\left(\begin{bmatrix}\boldsymbol{A} & \boldsymbol{P} \\ \boldsymbol{0} & \boldsymbol{S}\end{bmatrix} - \begin{bmatrix}\boldsymbol{G_1} \\ \boldsymbol{G_2}\end{bmatrix} \begin{bmatrix}\boldsymbol{C} & \boldsymbol{Q}\end{bmatrix}\right)$ are on the open left-half plane. In this paper, the pole assignment based on the interval linear matrix inequality method is applied to select the gain matrices $\boldsymbol{K}$ and $\boldsymbol{G}$.
5. *Construct the coordinated frequency controller*. The regulator issues in Equation (14) are solved and the solutions of matrices $\boldsymbol{\Pi}$ and $\boldsymbol{\Gamma}$ are found. Then, the observer is constructed as in Equation (17), and the error feedback controller in Equation (18) can be designed by the matrices $(\boldsymbol{F}, \boldsymbol{G}, \boldsymbol{H})$.
6. *Give the control orders*. Once the error feedback controller is constructed, the control input $\boldsymbol{u} \ = \left[\boldsymbol{\Delta P_{Grefi}}, \boldsymbol{\Delta P_{EALrefj}}\right]^{\mathrm{T}}$ is optimized at time t_k. Then, the optimal values of ΔP_{Grefi} and $\Delta P_{EALrefj}$ are transmitted to the control units of the thermal generators and EALs. Thus, the active power of the generation and demand sides are regulated to eliminate the frequency deviation in the isolated industrial microgrid.
7. *Repeat the above steps or finish*. Once the control objective is achieved, i.e., the frequency recovers to the normal value with the help of the proposed controller, the coordinated frequency control scheme is finished. Otherwise, repeat the above steps at the next time t_{k+1}.

In summary, once the proposed frequency control scheme is activated, the state variables $\boldsymbol{x}$, disturbance $\boldsymbol{d}$, and frequency deviation Δf in the isolated industrial microgrid are measured by the WAMS. Then, the coordinated frequency control model in Equation (10) is constructed as the foundation. After checking assumptions, selecting gain matrices, and solving regulator equations, the error feedback controller is designed by using the output regulation theory. Then, the optimized control inputs $\boldsymbol{u} \ = \left[\boldsymbol{\Delta P_{Grefi}}, \boldsymbol{\Delta P_{EALrefj}}\right]^{\mathrm{T}}$ are

obtained and given as the regulation commands to thermal generators and EALs, so that the output $\boldsymbol{y} = \Delta f$ can be eliminated by compensating for the power disturbance $\boldsymbol{d}$ caused by emergencies or wind power fluctuations. Based on that, the emergency frequency control problem is solved by applying the output regulation approach.

The effectiveness of the proposed frequency control scheme will be validated via time domain simulation in the next section.

5. Simulation Results

To validate the performance of the proposed coordinated frequency controller based on the output regulation approach, the isolated industrial microgrid presented in Figure 1 is taken as the study case, which is conducted on the real-time digital simulation (RTDS) platform and in MATLAB. The RTDS was developed for the electromagnetic transient simulation of power systems based on the real-time hardware computation platform. The synchronous generator model in the RTDS platform was applied for the simulation of thermal generators in the industrial microgrid. An aggregated model of a 2-MW doubly fed induction generator (DFIG) was used to represent wind farms based on the modeling method presented in [32]. The EALs were conducted, as in Figure 4, with the controllable load function in the RTDS platform.

When the coordinated frequency control strategy is activated, the state variables $\boldsymbol{x}$, disturbance $\boldsymbol{d}$, and error $\boldsymbol{e}$ of the industrial microgrid are collected and then transmitted to MATLAB during each time step. Thus, the error feedback controller in Equation (18) is calculated in MATLAB based on the procedures provided in Section 4.2, and the control input $\boldsymbol{u}$ is fed into the RTDS platform. Consequently, the thermal generator and EAL models will carry out the frequency control scheme as the optimized control input $\boldsymbol{u}$, which means that the output power of the thermal generators and EALs will be regulated to achieve error tracking. The whole simulation process between the RTDS platform and MATLAB, shown in Figure 7, will repeat in the next time step.

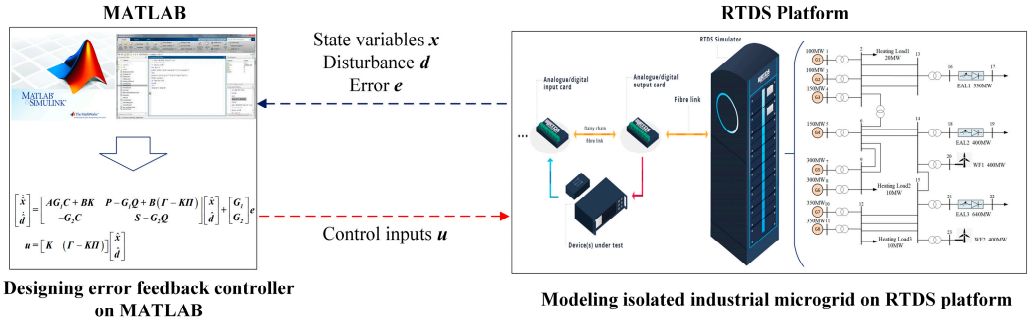

Figure 7. The simulation process between the RTDS platform and MATLAB.

The installed capacity of the generators and the power demand of the EALs are listed in Tables 1 and 2. In this section, we consider two cases, i.e., the "N-1" and wind power fluctuation scenarios, to verify the effectiveness and robustness of the coordinated frequency control scheme. To further prove the improved performance of the proposed control scheme, PI control methods are also conducted as a comparison.

5.1. "N-1" Scenario

In this case, the selected typical working situation of the industrial microgrid is listed in Table 3. The wind power fluctuates within a slight range of less than 1% of the installed wind farm capacity, which can be covered by the ESSs equipped in the wind farms. As mentioned in Section 2, the isolated industrial microgrid operation is supposed to meet the "N-1" principle. Therefore, we considered a more severe situation than in Section 2 (where G5 is out of service) so to verify the performance of the proposed coordinated frequency control scheme. In this case, the thermal generator G7 is tripped off due to a short-circuit

fault at t = 2 s, leading to an active imbalance of 191.5 MW. The control strategies applied in this case are presented in Table 5.

Table 5. The control schemes in "N-1" scenarios.

Control Strategy	Method
Strategy A	Only primary frequency control on the rest of the thermal generators
Strategy B	Load-shedding strategy on EAL1
Strategy C	PI control methods on the generators and EALs
Strategy D	Proposed coordinated frequency control

In Strategy A, the power disturbance of 191.5 MW is only compensated by the primary frequency reserve of 72.5 MW from the rest of the thermal generators. With the traditional load-shedding strategy, the EAL1 of 330 MW is shed as a whole part in Strategy B, as mentioned in Section 2. The PI-based control strategy is designed by using the frequency deviation Δf for the thermal generators and EALs. The signal of Δf is collected and given as the input of the PI controllers. Then, the active power regulation of the thermal generators and EALs, ΔP_{Grefi} and $\Delta P_{EALrefj}$, can be calculated as follows:

$$\begin{aligned} \Delta P_{Grefi}(s) &= \left(K_{GPi} + \frac{K_{GIi}}{s}\right)\Delta f(s) \\ \Delta P_{EALrefj}(s) &= \left(K_{LPj} + \frac{K_{LIj}}{s}\right)\Delta f(s) \end{aligned} \tag{24}$$

where K_{GPi} and K_{GIi}, and K_{LPj} and K_{LIj}, are the gain coefficients of the PI controllers for the thermal generators and EALs, with the setting methods introduced in [33,34].

The simulation results are demonstrated in Figure 8. When the thermal generator G7 is out of service, the primary frequency reserve capacity from the rest of the generators is apparently insufficient for the active power imbalance, leading to the frequency collapse of the industrial microgrid within 30 s, as shown in Figure 8a. The total power deviations of the thermal generators and EALs are demonstrated in Figures 8b and 8c, respectively.

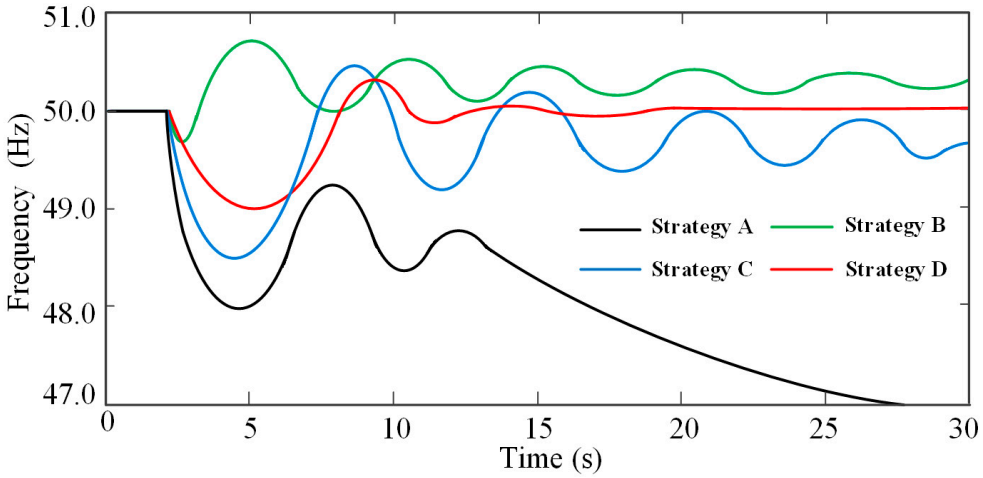

(**a**)

Figure 8. *Cont.*

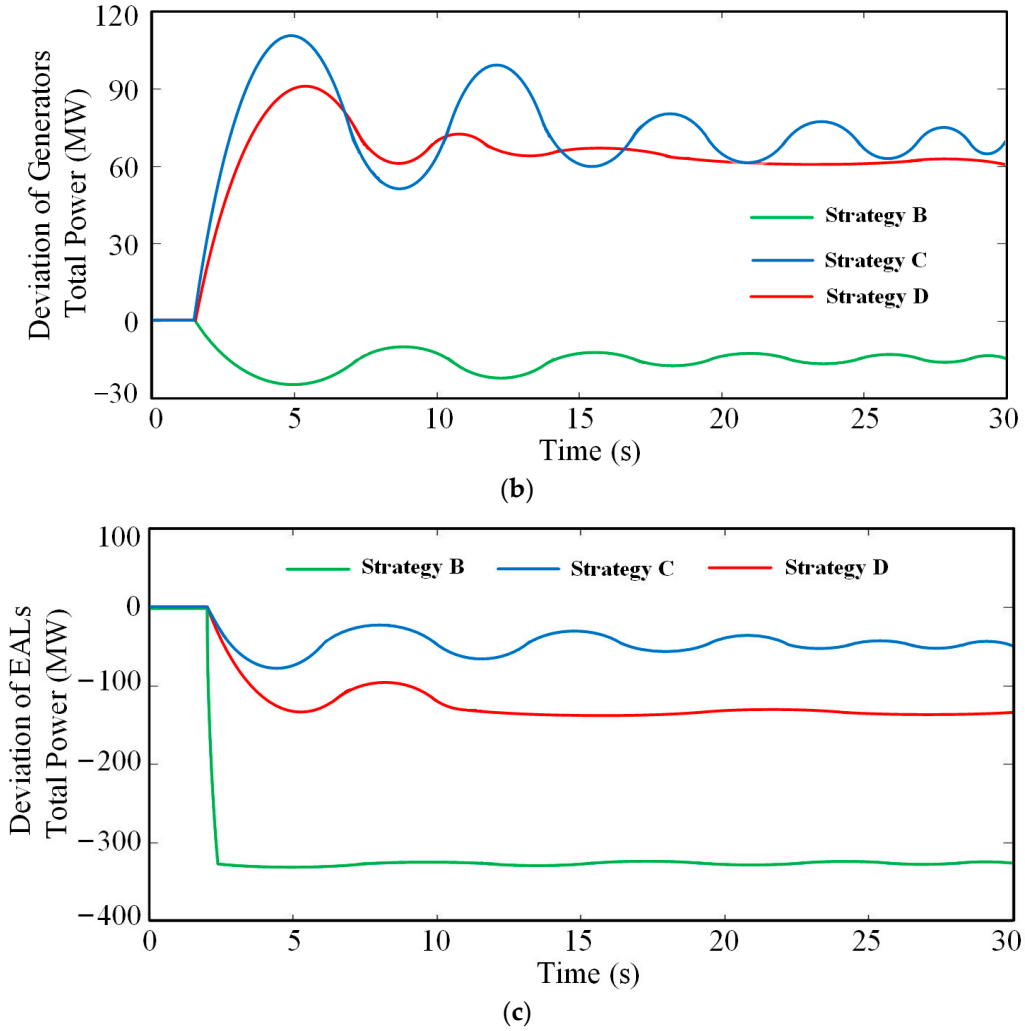

Figure 8. Simulation results of applying different control strategies in the "N-1" scenario, where G7 is tripped off. (**a**) The frequency response; (**b**) The total power deviation of the generators; (**c**) The total power deviation of the EALs.

Due to the large installed capacity of single aluminum production lines, the shedding of EAL1 of 330 MW is much higher than the active power disturbance. As a result, the frequency with Strategy B rises to over 50.5 Hz, which is not allowed for the industrial microgrid operation. When the PI control method is used on the generators and EALs, the industrial microgrid frequency decreases to 48.5 Hz at t = 4 s. Although the active power balance is able to be compensated by the generation and demand sides to a certain extent, the power reserve distribution among the generators and EALs is ambiguous because it lacks coordination with the PI controllers. Therefore, the PI control strategy presents an unsatisfactory robustness when reflecting on the frequency fluctuation within a certain range.

When the coordinated frequency control scheme is applied in Strategy D, the frequency response, such as the ROCOF and nadir, are obviously improved when compared to Strategies B and C. In addition, the frequency response presents a much stabler way to recover the normal working value. As discussed in Section 3, the EALs can be regulated from over −0.9 p.u. to 1.05 p.u. of the installed capacity. By virtue of the fast response, the EALs provide a reserve capacity of about 130 MW after G7 is out of service, preventing the further decrease in the frequency. The thermal generators provide a power reserve of about 90 MW in total. Then, under the coordination between the generators and EALs, the microgrid frequency recovers to 50 Hz within 20 s. Therefore, the proposed coordinated

frequency control strategy is effective in restoring the frequency to a normal value when emergencies occur, which is significant for guaranteeing the frequency stability of the isolated industrial microgrid.

5.2. Wind Power Fluctuation Scenario

As presented in Table 3, the installed capacity of the wind power is about 30% of the total generation capacity in the industrial microgrid. Therefore, the influence of wind power fluctuation on the microgrid frequency control is studied. Normally, wind farms are equipped with ESSs; however, here, we consider a severe scenario with an extreme short-term wind power fluctuation without any assistance from the ESS.

Total wind power fluctuation in a period of 600 s is demonstrated in Figure 9, and the maximum deviation of the total wind power reaches about 180 MW. Due to the intermittency and variability of the wind power, the industrial microgrid frequency fluctuates as well, which is unsatisfactory for the frequency stability.

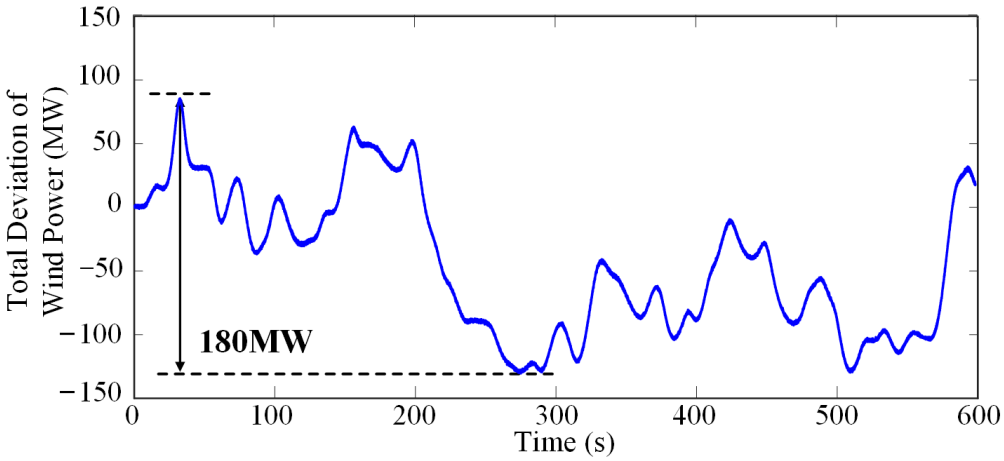

Figure 9. The total wind power fluctuation in a period of 600 s.

The control strategies applied in this case are presented in Table 5. Figure 10 illustrates the simulation results of the frequency response of different control strategies. With the primary frequency control of the generators, the frequency deviation caused by the wind power fluctuation changes from over −0.5 Hz to 0.3 Hz, which is not safe for the operation of the industrial microgrid. With the help of the PI control strategy, the wind power fluctuation can be partly compensated by the thermal generators and EALs. As a result, the frequency deviation is able to be restricted to ±0.3 Hz, which presents a positive effect of dealing with a power imbalance.

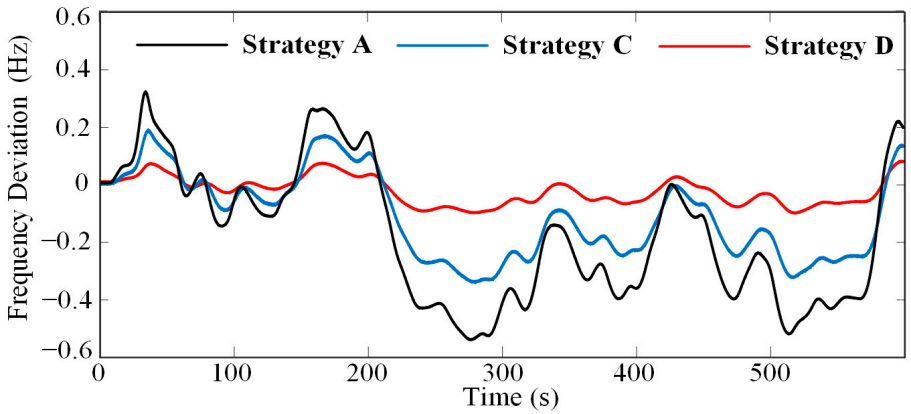

Figure 10. The frequency response with different control strategies.

Compared with the PI control method, the coordinated frequency control strategy shows a better performance in smoothing the intensive wind power fluctuation. Consequently, the frequency fluctuates within ±0.1 Hz by virtue of the rapid response of the EALs. The power deviation of the generators and EALs are demonstrated in Figure 11. The power deviation of the EALs reach to about 160 MW, while the thermal generators provide a power reserve of less than 30 MW for the wind power fluctuation, revealing that the wind power fluctuation is mainly compensated by the EALs instead of the generators. The proposed coordinated control scheme presents a satisfactory robustness against the wind power fluctuation, guaranteeing a stable frequency for the industrial microgrid.

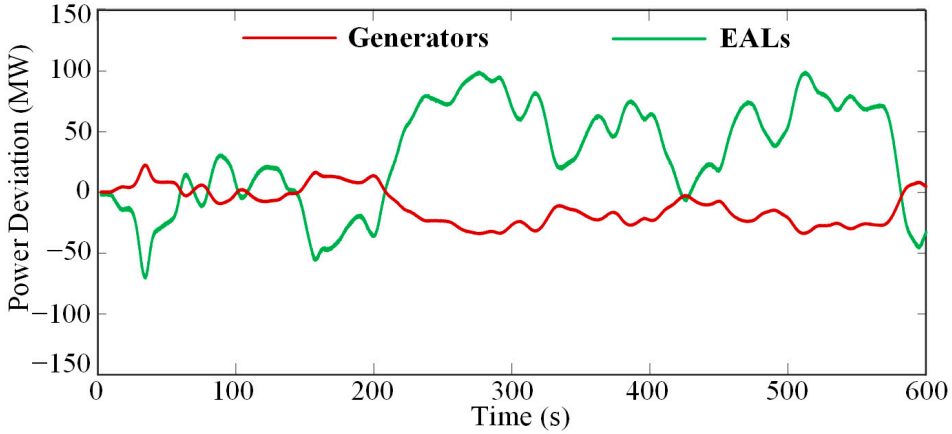

Figure 11. The power deviation of the generators and EALs with the coordinated frequency control strategy.

6. Discussion and Conclusions

This paper studied emergency frequency control issues in an actual isolated aluminum production industrial microgrid with a high proportion of wind power. As a type of high-energy-consuming industrial load, the EAL shows great potential for power regulation due to the fast response and huge capacity, which is able to participate in the frequency control of the industrial microgrid. The regulation method and control model of the EAL have been investigated in this work. On the basis of that, a coordinated frequency control model which combines the thermal generators and EALs was developed to deal with emergency scenarios in the microgrid. The coordinated frequency control issue was formulated as an output regulation problem. With the help of the output regulation theory, the error feedback controller for the isolated industrial microgrid was designed to regulate the output power of the generators and EALs, achieving coordinated frequency control when a large power disturbance occurs.

Compared with the traditional PI controller, the main advantages of the error feedback controller include the tracking of the power disturbance $\boldsymbol{d}$ and the achievement of steady error regulation ($\lim_{t\to\infty} \boldsymbol{e}(t) = 0$). As a type of model-based controller, the error feedback controller guarantees more desirable control effects in terms of frequency recovery. However, the limitations of the proposed approach in practical applications are also obvious, which mainly focus on the time-delay issues of the WAMS. The communication and operational delays might present a negative impact on the control effects. In practical applications, the evaluation model of the communication delay was applied so to decrease the negative effects. The operational delay also needs to be measured and analyzed in the process of designing the error feedback controller.

The simulation results conducted on the actual industrial microgrid have illustrated the following conclusions:

1. The proposed coordinated frequency control strategy is able to realize frequency recovery to normal values in a short amount of time in the presence of a large power imbalance.

2. Compared with the PI control method, the proposed frequency control method based on the output regulation approach presents better effectiveness in frequency recovery and robustness against the wind power fluctuations.
3. The EALs present a much faster response than the thermal generators in smoothing wind power fluctuations, which is applicable to improving the frequency stability in extreme emergency scenarios.

In summary, by developing the regulation potential of EALs, the proposed coordinated frequency control scheme based on output regulation theory presents satisfactory effectiveness and robustness in dealing with power disturbances caused by emergencies and wind power fluctuations, which significantly improves the frequency reliability and stability in industrial microgrids.

The working constraints on thermal generators and EALs, such as the regulating ratio and production limitations, may influence the practical control effect of the coordinated frequency control scheme based on the output regulation approach. Future studies will focus on the further optimization of the regulation between the generators and EALs so to achieve lower control costs. In addition, time-delay issues will be considered for the practical applications of the proposed frequency control scheme so to achieve the more accurate online computation of the power reserve distribution.

Author Contributions: Conceptualization, X.D. and S.Z.; methodology, X.D.; software, X.D.; validation, X.D. and S.Z.; formal analysis, X.D.; investigation, S.Z.; resources, X.D.; data curation, X.D.; writing—original draft preparation, S.Z.; writing—review and editing, X.D.; visualization, X.D.; supervision, X.D.; project administration, X.D.; funding acquisition, X.D. All authors have read and agreed to the published version of the manuscript.

Funding: This work was supported by the Technology Project of China Southern Power Grid (0500002022030301GH00163).

Data Availability Statement: Data are available on request from the corresponding author rather than via direct availability.

Conflicts of Interest: Author Sujie Zhang was employed by the State Grid Shanghai Municipal Electric Power Company, and remaining authors declare that no conflicts of interest.

References

1. Wei, Y.; Chen, K.; Kang, J.; Chen, W.; Wang, X.; Zhang, X. Policy and management of carbon peaking and carbon neutrality: A literature review. *Engineering* **2022**, *14*, 52–63. [CrossRef]
2. Zhuang, G.; Zhou, H.; Ni, W. *China's Road to Carbon Peaking and Carbon Neutrality*; Springer: Singapore, 2023; pp. 1–20.
3. Xu, B. Exploring the sustainable growth pathway of wind power in China: Using the semiparametric regression model. *Energy Policy* **2023**, *183*, 113845. [CrossRef]
4. National Energy Administration Released the Statistical Data of the National Power Industry in 2023. Available online: https://www.nea.gov.cn/2024-01/26/c_1310762246.htm (accessed on 26 January 2024).
5. Liao, S.; Xu, J.; Sun, Y.; Bao, Y. Local utilization of wind electricity in isolated power systems by employing coordinated control scheme of industrial energy-intensive load. *Appl. Energy* **2018**, *217*, 14–24. [CrossRef]
6. Li, H.; Eseye, A.T.; Zhang, J.; Zheng, D. Optimal energy management for industrial microgrids with high-penetration renewables. *Prot. Control Mod. Power Syst.* **2017**, *2*, 12. [CrossRef]
7. Wang, Z.; Yang, B.; Wei, W.; Zhu, S.; Guan, X.; Sun, D. Multi-Energy Microgrids: Designing, operation under new business models, and engineering practices in China. *IEEE Electrif. Mag.* **2021**, *9*, 75–82. [CrossRef]
8. Fernández-Guillamón, A.; Gómez-Lázaro, E.; Muljadi, E.; Molina-García, Á. Power systems with high renewable energy sources: A review of inertia and frequency control strategies over time. *Renew. Sustain. Energy Rev.* **2019**, *115*, 109369. [CrossRef]
9. Mohandes, B.; El Moursi, M.S.; Hatziargyriou, N.; El Khatib, S. A review of power system flexibility with high penetration of renewables. *IEEE Trans. Power Syst.* **2019**, *34*, 3140–3155. [CrossRef]
10. Davari, M.; Gao, W.; Jiang, Z.-P.; Lewis, F.L. An optimal primary frequency control based on adaptive dynamic programming for islanded modernized microgrids. *IEEE Trans. Autom. Sci. Eng.* **2020**, *18*, 1109–1121. [CrossRef]
11. Mottaghizadeh, M.; Aminifar, F.; Amraee, T.; Sanaye-Pasand, M. Distributed robust secondary control of islanded microgrids: Voltage, frequency, and power sharing. *IEEE Trans. Power Deliv.* **2021**, *36*, 2501–2509. [CrossRef]
12. Wang, C.; Mei, S.; Dong, Q.; Chen, R.; Zhu, B. Coordinated load shedding control scheme for recovering frequency in islanded microgrids. *IEEE Access* **2020**, *8*, 215388–215398. [CrossRef]

13. Li, J.; Chen, S.; Wang, X.; Pu, T. Load shedding control strategy in power grid emergency state based on deep reinforcement learning. *CSEE J. Power Energy* **2021**, *8*, 1175–1182.
14. Yu, L.; Wu, J.; Cheng, Y.; Meng, G.; Chen, S.; Lu, Y.; Xu, K. Control Strategy for Wind Farms-Energy Storage Participation in Primary Frequency Regulation Considering Wind Turbine Operation State. *Energies* **2024**, *17*, 3547. [CrossRef]
15. Arrigo, F.; Bompard, E.; Merlo, M.; Milano, F. Assessment of primary frequency control through battery energy storage systems. *Int. J. Electr. Power Energy Syst.* **2020**, *115*, 105428. [CrossRef]
16. Jiang, H.; Lin, J.; Song, Y.; Gao, W.; Xu, Y.; Shu, B.; Li, X.; Dong, J. Demand side frequency control scheme in an isolated wind power system for industrial aluminum smelting production. *IEEE Trans. Power Syst.* **2013**, *29*, 844–853. [CrossRef]
17. Xu, J.; Liao, S.; Sun, Y.; Ma, X.; Gao, W.; Li, X.; Gu, J.; Dong, J.; Zhou, M. An isolated industrial power system driven by wind-coal power for aluminum productions: A case study of frequency control. *IEEE Trans. Power Syst.* **2014**, *30*, 471–483. [CrossRef]
18. Ding, X.; Xu, J.; Sun, Y.; Liao, S.; Zheng, J. A demand side controller of electrolytic aluminum industrial microgrids considering wind power fluctuations. *Prot. Control Mod. Power Syst.* **2022**, *7*, 49. [CrossRef]
19. Liao, S.; Xu, J.; Sun, Y.; Bao, Y.; Tang, B. Control of energy-intensive load for power smoothing in wind power plants. *IEEE Trans. Power Syst.* **2018**, *33*, 6142–6154. [CrossRef]
20. Bao, Y.; Xu, J.; Feng, W.; Sun, Y.; Liao, S.; Yin, R.; Jiang, Y.; Jin, M.; Marnay, C. Provision of secondary frequency regulation by coordinated dispatch of industrial loads and thermal power plants. *Appl. Energy* **2019**, *241*, 302–312. [CrossRef]
21. Babahajiani, P.; Shafiee, Q.; Bevrani, H. Intelligent demand response contribution in frequency control of multi-area power systems. *IEEE Trans. Smart Grid* **2016**, *9*, 1282–1291. [CrossRef]
22. Zhao, J.; Lyu, X.; Fu, Y.; Hu, X.; Li, F. Coordinated microgrid frequency regulation based on DFIG variable coefficient using virtual inertia and primary frequency control. *IEEE Trans. Energy Convers.* **2016**, *31*, 833–845. [CrossRef]
23. Jiang, H.; Lin, J.; Song, Y.; Hill, D.J. MPC-based frequency control with demand-side participation: A case study in an isolated wind-aluminum power system. *IEEE Trans. Power Syst.* **2014**, *30*, 3327–3337. [CrossRef]
24. Xu, J.; Fu, H.; Liao, S.; Xie, B.; Ke, D.; Sun, Y.; Li, X.; Peng, X. Demand-side management based on model predictive control in distribution network for smoothing distributed photovoltaic power fluctuations. *J. Mod. Power Syst. Clean Energy* **2022**, *10*, 1326–1336. [CrossRef]
25. Cui, T.; Lin, W.; Sun, Y.; Xu, J.; Zhang, H. Excitation voltage control for emergency frequency regulation of island power systems with voltage-dependent loads. *IEEE Trans. Power Syst.* **2015**, *31*, 1204–1217. [CrossRef]
26. Zhao, H.; Hong, M.; Lin, W.; Loparo, K.A. Voltage and frequency regulation of microgrid with battery energy storage systems. *IEEE Trans. Smart Grid* **2017**, *10*, 414–424. [CrossRef]
27. Sun, Y.; Lin, J.; Song, Y.; Xu, J.; Li, X.; Dong, J. An industrial system powered by wind and coal for aluminum production: A case study of technical demonstration and economic feasibility. *Energies* **2012**, *5*, 4844–4869. [CrossRef]
28. Principles of the Hall-Héroult Process. Available online: http://www.peter-entner.com/e/theory/PrincHH/PrincHH.aspx (accessed on 26 January 2005).
29. Bao, Y.; Xu, J.; Liao, S.; Sun, Y.; Li, X.; Jiang, Y.; Ke, D.; Yang, J.; Peng, X. Field verification of frequency control by energy-intensive loads for isolated power systems with high penetration of wind power. *IEEE Trans. Power Syst.* **2018**, *33*, 6098–6108. [CrossRef]
30. Isidori, A.; Byrnes, C.I. Output regulation of nonlinear systems. *IEEE Trans. Autom. Control* **1990**, *35*, 131–140. [CrossRef]
31. Phadke, A.G.; Bi, T. Phasor measurement units, WAMS, and their applications in protection and control of power systems. *J. Mod. Power Syst. Clean Energy* **2018**, *6*, 619–629. [CrossRef]
32. Fernández, L.M.; Jurado, F.; Saenz, J.R. Aggregated dynamic model for wind farms with doubly fed induction generator wind turbines. *Renew. Energy* **2008**, *33*, 129–140. [CrossRef]
33. Sönmez, S.; Ayasun, S. Stability region in the parameter space of PI controller for a single-area load frequency control system with time delay. *IEEE Trans. Power Syst.* **2015**, *31*, 829–830. [CrossRef]
34. Jiang, L.; Yao, W.; Wu, Q.; Wen, J.; Cheng, S. Delay-dependent stability for load frequency control with constant and time-varying delays. *IEEE Trans. Power Syst.* **2011**, *27*, 932–941. [CrossRef]

Disclaimer/Publisher's Note: The statements, opinions and data contained in all publications are solely those of the individual author(s) and contributor(s) and not of MDPI and/or the editor(s). MDPI and/or the editor(s) disclaim responsibility for any injury to people or property resulting from any ideas, methods, instructions or products referred to in the content.